PIER Letters

(Received 9 January 2026, Accepted 26 February 2026, Scheduled 12 March 2026)

A Low-Profile Polarization Conversion Metasurface Array Antenna with Broadband RCS Reduction

Jinhua Tian, Xutong Wang, Zixin Liang, Yuzhen Gao, Chunting Wang, and Liping Han*

College of Physics and Electronic Engineering, Shanxi University, Taiyuan 030006, China

ABSTRACT: A novel integration method of a polarization conversion metasurface (PCM) and an array antenna for radar cross-section (RCS) reduction is presented. This method combines the PCM with a slot array antenna operating at 11.5 GHz for reducing RCS. The metasurface is composed of polarization conversion units arranged in a checkerboard pattern, and each PCM unit cell is made up of two symmetrical fork-shaped structures. The polarization conversion units can achieve a polarization conversion ratio (PCR) of over 90% in the frequency band of 10.12–19.93 GHz (65%). The measurements demonstrate that the antenna attains over 10 dB RCS reduction in the frequency range of 9.9–20.7 GHz (71%). Meanwhile, the radiation performance of the antenna is effectively preserved.

1. INTRODUCTION

With the rapid development of modern electronic technology, the requirement for stealth capabilities has been significantly enhanced [1]. It is a key method to reduce the radar cross-section (RCS) for achieving electromagnetic stealth. The widespread application of low RCS antennas is attributed to their characteristics such as wide bandwidth performance, simple structure, light weight, and controllable radiation [2–4]. A range of methods have been explored to reduce the RCS of antennas [5–9], such as coding metasurfaces, absorbing metasurfaces, artificial magnetic conductors (AMC), and polarization conversion metasurfaces (PCMs). In [10], a coding metasurface based on low-Q resonators is proposed to achieve wideband RCS reduction. In [11], a hybrid absorptive-diffusive frequency selective reflector is developed for a wideband low-RCS antenna. In [12], a periodic artificial magnetic conducting (AMC) metasurface using phase cancellation technology is applied to achieve wideband RCS reduction. In [13], polarization conversion metasurfaces are investigated as a promising strategy for antenna RCS reduction.

Due to the flexibility of the PCM, it has attracted the attention of scholars in the field of low RCS antennas [14–17]. Over the past decade, diverse metasurfaces have been adopted for reducing the RCS of antennas. In [18], a PCM composed of curved square ring-shaped units is arranged around a radiation patch, achieving a 10 dB RCS reduction bandwidth of 7.05%. In [19], a PCM constructed from square PCM units with two diagonal slits is proposed, and it is combined with a 4×4 array antenna, with the measured bandwidth of 10 dB RCS reduction reaching 22.6%. In [20], a PCM is composed of circular polarization conversion units arranged in a checkerboard pattern, and the metasurface is applied to multiple-input multiple-output (MIMO) antennas. The relative bandwidth is 35.3%. In [21] and [22], the metasurface consists of double rhombus-shaped and dumbbell-shaped polarization conversion units, respectively. The metasurface and its mirror image units are arranged on the slot antenna. The 10 dB RCS reduction bandwidths can reach 44% and 46%, respectively. In [23], the metasurface composed of fishbone-shaped polarization conversion units is combined with a slot array antenna. The final 10 dB RCS reduction bandwidth attains 51.9%. In [24], dual-headed arrow-shaped PCM units are loaded around a circularly polarized (CP) patch antenna in the four quadrants, delivering a 10 dB RCS reduction bandwidth of 53.9%. In [25], a low-profile broadband C-band antenna is designed, which achieves a 40% bandwidth for 10 dB RCS reduction. In [26], the low RCS characteristic is achieved by using PCM and partial reflection surface (PRS), and its 10 dB RCS reduction bandwidth attains 75.8%. In [27], a wideband and low-RCS circularly polarized patch antenna is proposed, and the impedance bandwidth is 13.65%. In [28], a low-profile and high-gain planar dipole antenna integrated with orthogonally arranged bowtie-shaped PCMs is proposed, and the 10 dB RCS reduction bandwidth reaches 33.88%. In addition, the RCS reduction bandwidth is expanded by using a cross configuration [29]. The aforementioned antennas can reduce RCS while maintaining excellent radiation performance. However, it is still a significant challenge to realize a broader RCS reduction bandwidth with a low profile.

In this work, a low-profile PCM array antenna is demonstrated. It consists of a slot array antenna and a checkerboard metasurface. The checkerboard configuration creates a 180° phase difference of reflected waves between the PCM and mirror array, and the measured data illustrate that the 10 dB RCS reduction bandwidth is 71%. It has the advantages of broadband RCS reduction (71.7%), ultra-low profile (3.4 mm, $0.127\lambda_0$), and low cost (FR4 substrate), which is suit-

* Corresponding author: Liping Han (hlp@sxu.edu.cn).

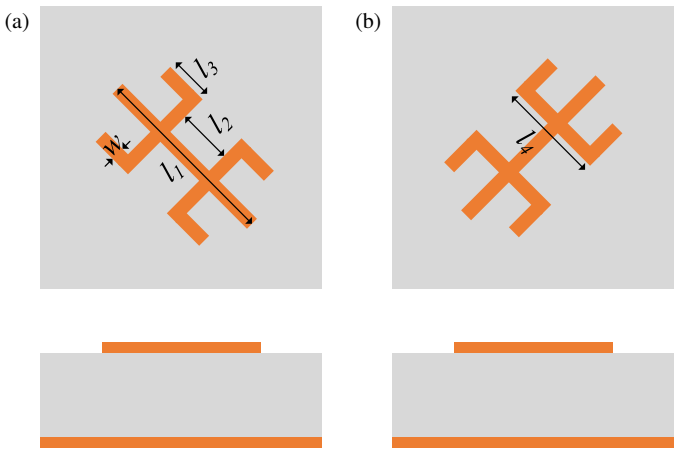

FIGURE 1. Schematic of PCM unit cell. (a) PCM unit. (b) Mirror unit.

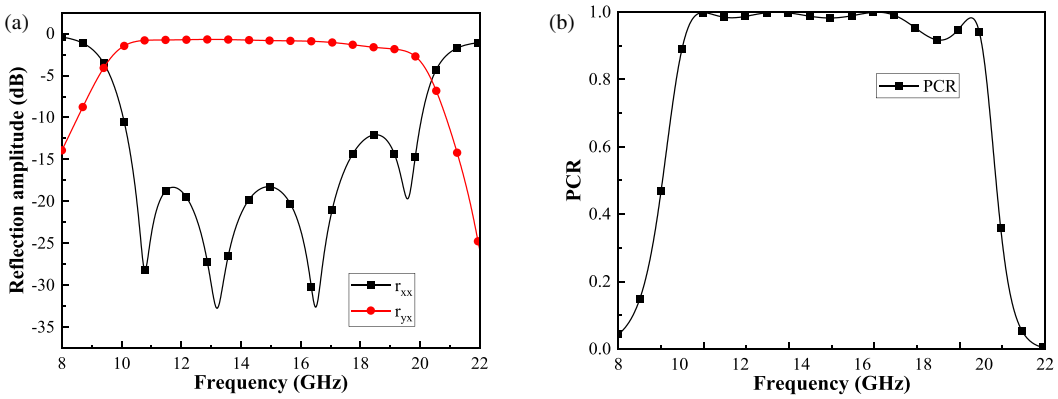

FIGURE 2. (a) Reflection coefficients of co- and cross- polarizations. (b) PCR.

able for practical applications in X/Ku-band electromagnetic stealth systems.

2. CHECKERBOARD PCM

A PCM unit cell is designed and analyzed first, and then the PCM and its mirror units are arranged in a checkerboard configuration to form the metasurface.

2.1. PCM Unit Cells

Figure 1 shows the structure of the PCM and its mirror unit. The upper layer of the substrate is composed of two symmetrical fork-shaped strips. The lower layer of the substrate is grounded with metallic copper. The unit cell exhibits dimensions of 8 mm × 8 mm × 2.4 mm. FR4 is selected as the dielectric substrate, with a thickness of 2.4 mm, a tangent loss of 0.025, and a relative permittivity of 4.3. The optimized parameters simulated by software CST STUDIO SUITE 2020 are: $l_1 = 0.9$ mm, $l_2 = 6$ mm, $l_3 = 5$ mm, $l_4 = 5$ mm, and $w_1 = 0.8$ mm.

The polarization conversion ratio (PCR) is a crucial indicator for measuring the ability of polarization rotation (PR), as described in [30]. For a normally incident y-polarized EM wave, the PCR is defined as $r_{xy}^2/(r_{xy}^2 + r_{yy}^2)$, where r_{yy} and r_{xy} represent the co- and cross-polarization reflection coefficients, respectively. Figure 2(a) shows the co- and cross-polarization reflection coefficients of the PCM unit. It can be seen that a wide cross-polarization conversion band from 10.05 to 20.06 GHz is obtained, within the range where the co-polarization reflection coefficient is lower than −10 dB. Figure 2(b) displays the PCM unit's PCR, which is over 90% in the 10.12–19.93 GHz band.

2.2. Chessboard PCM

The checkerboard PCM is demonstrated in Figure 3(a). It is made up of 2 × 2 PCM subarrays, and each subarray includes 4 × 4 PCM or their mirror units. The PCM is divided into four quadrants. The first and fourth quadrants consist of PCM units, while the second and third quadrants have their mirror-image units. The metasurface has an overall size of 64 mm × 64 mm × 2.4 mm. A metal plate is employed as the reference plane. The surface current distributions on the PCM are also investigated. Figure 3(b) plots the simulated current distributions at the resonant frequency. It is clear that the current directions of the PCM and its mirror unit are opposite, resulting in a phase difference of approximately 180°.

Figure 4 presents the monostatic RCS values of the PCM, as well as the RCS reduction results in comparison with the PEC reference. It can be observed that the RCS reduction performances for x- and y-polarized waves are basically consis-

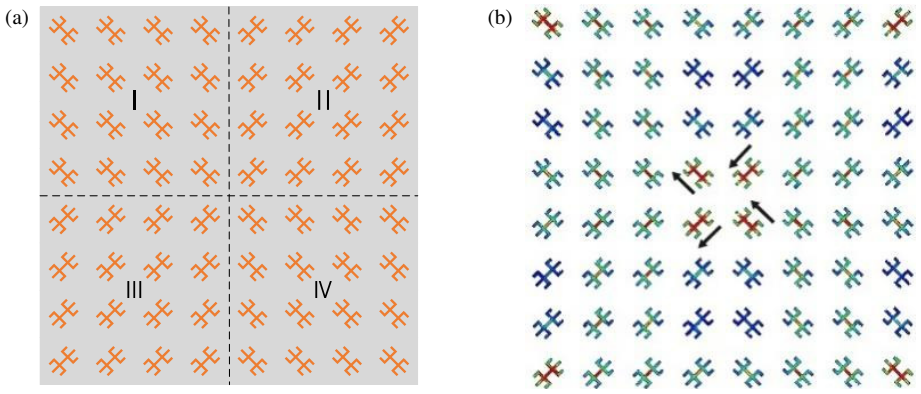

FIGURE 3. (a) Schematic of the PCM. (b) Surface current distribution.

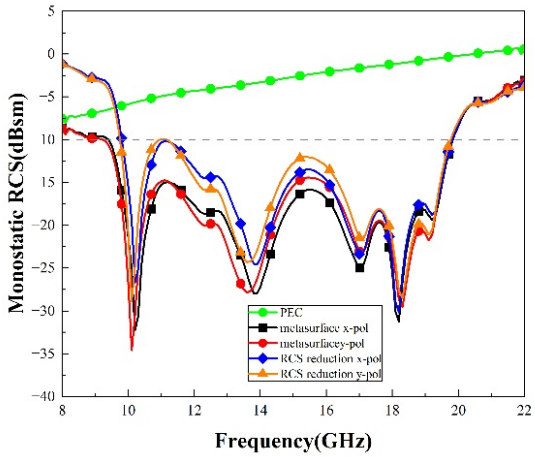

FIGURE 4. Monostatic RCS and RCS reduction.

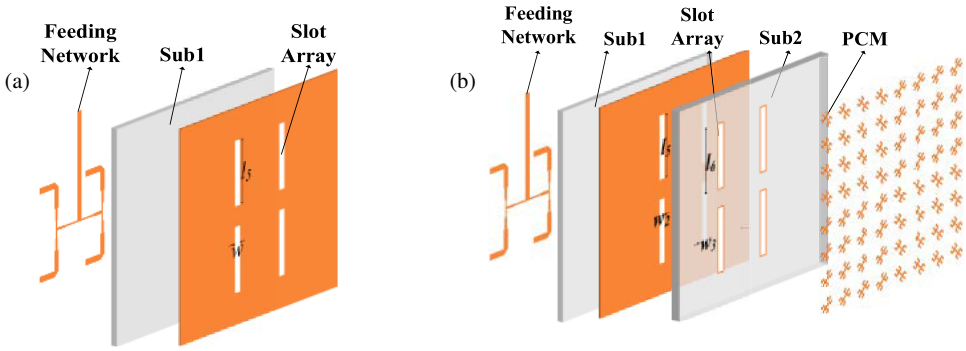

FIGURE 5. Schematic of (a) SAA, (b) PCM-SAA.

tent. Moreover, the 10 dB RCS reduction bandwidth covers 9.8–19.7 GHz, while the simulated RCS reduction value peaks at 10.2, 13.9, 17.1, and 18.2 GHz.

3. ARRAY ANTENNA WITH BROADBAND RCS REDUCTION

In this section, the PCM array is loaded onto a slot array antenna (SAA) to form the proposed antenna (PCM-SAA). The radiation and scattering performances are investigated.

3.1. Array Antenna Structure

The structure of the SAA is depicted in Figure 5(a). A metal plate with 4 rectangular slots is etched on the top surface of the substrate, with the slot length (l_5) of 19.5 mm and the width (w_2) of 1.6 mm. The feeding network is printed on the bottom side of the substrate. FR4 is chosen as the substrate. Figure 5(b) illustrates the configuration of the PCM-SAA composed of SAA and PCM. The overall size of the PCM-SAA is 64 mm × 64 mm × 3.4 mm. To reduce the coupling between the PCM and SAA, four slots are etched on the substrate of the

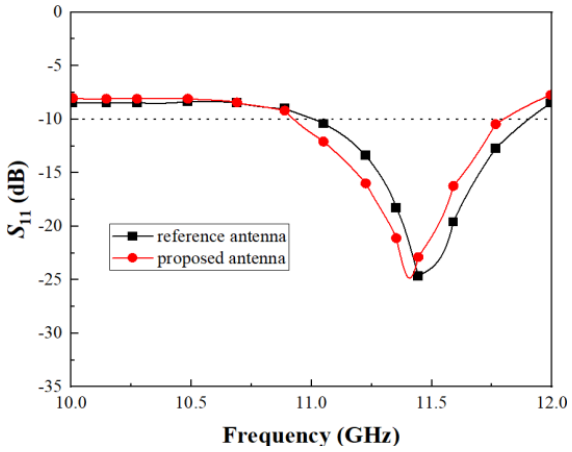

FIGURE 6. Simulated S_{11}.

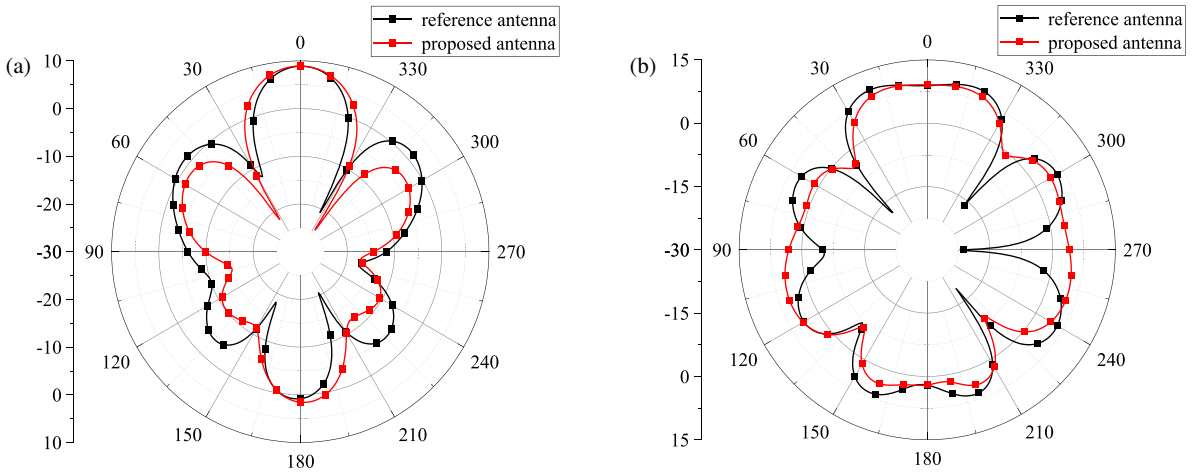

FIGURE 7. Radiation patterns of SAA and PCM-SAA at 11.5 GHz. (a) E-plane. (b) H-plane.

PCM, rather than on that of the SAA. The length (l_6) and width (w_3) of the slot on the PCM substrate are 21.3 mm and 2.4 mm.

3.2. Radiation Performance

The simulated reflection coefficients of the SAA and PCM-SAA are displayed in Figure 6. It is obvious that the operating bands of the SAA and PCM-SAA are 11–11.85 GHz (7.4%) and 10.9–11.76 GHz (7.6%), respectively. Compared with the SAA, the resonant frequency of the PCM-SAA is slightly shifted to a lower frequency, and the operating band is expanded by 0.58 GHz.

Figure 7 shows the simulated E- and H-plane radiation patterns of the SAA and PCM-SAA at 11.5 GHz. It can be seen that the patterns of the PCM-SAA agree well with those of SAA. The main lobes are all oriented along the normal direction in both planes. The results demonstrate that the radiation performance is well preserved after incorporating the PCM. The simulated peak gains of the SAA and PCM-SAA are 6.8 dB and 5.3 dB, respectively.

3.3. Scattering Performance

The monostatic RCS and RCS reduction results of the SAA and PCM-SAA at normal incidence are shown in Figure 8. Under x-polarized incidence, the PCM-SAA achieves a 10 dB RCS reduction bandwidth of 10.1–20.3 GHz (67.1%), with the maximum RCS reduction of 28 dB achieved at 19.5 GHz. The 10 dB RCS reduction under y-polarized incidence spans 9.9–20.2 GHz (68.4%), and the maximum reduction here attains 44 dB at 13.2 GHz.

The bistatic RCS curves of the SAA and PCM-SAA are exhibited in Figure 9. It is evident that the RCS reduction of the PCM-SAA is 18 dB, and the RCS reduction effect can be realized between $-38°$ and $+38°$. Due to the phase cancellation among the reflected waves from the checkerboard PCM, the reflected energy is scattered into directions away from the boresight, thereby suppressing backscattering along the normal direction.

4. EXPERIMENT RESULTS

Figure 10(a) depicts the pictures of the manufactured antennas. The measurement setup is illustrated in Figure 10(b), where two

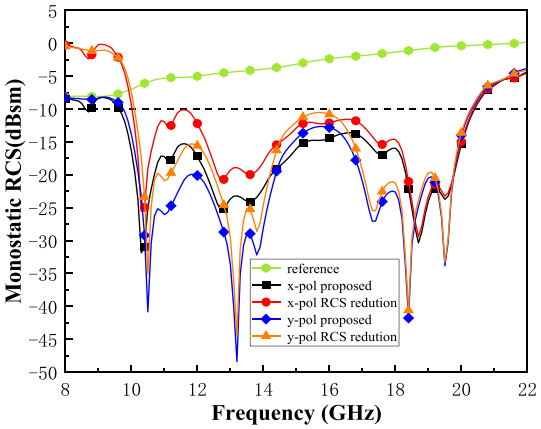

FIGURE 8. Monostatic RCS and reduction of antennas.

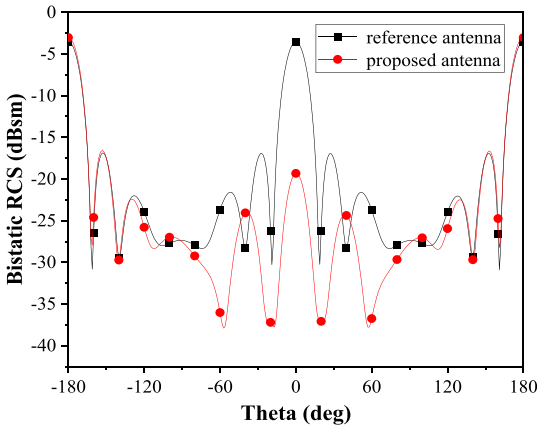

FIGURE 9. The bistatic RCS curves of SAA and PCM-SAA.

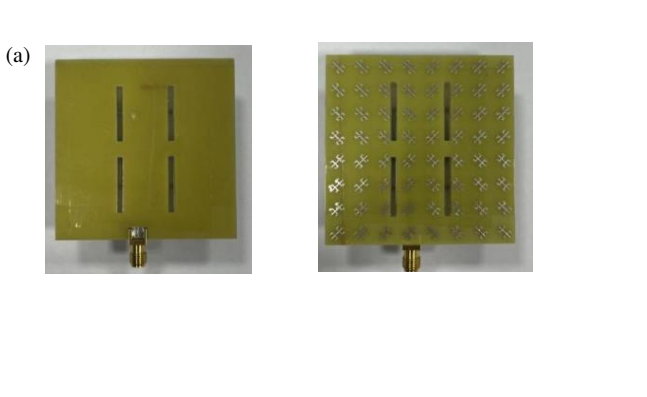

FIGURE 10. (a) Photos of SAA and PCM-SAA. (b) RCS measurement setup.

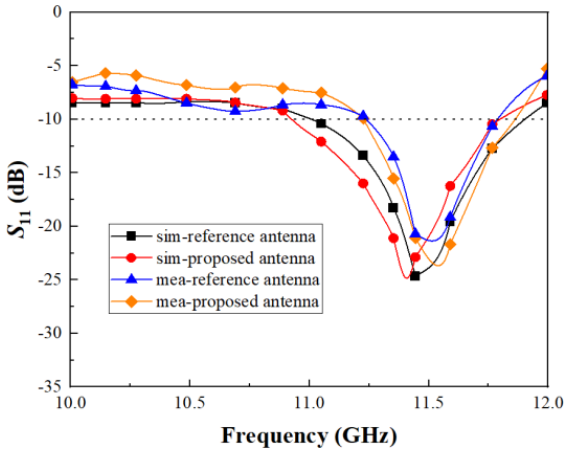

FIGURE 11. Simulated and measured S_{11} of SAA and PSA.

horn antennas act as the transmitting and receiving antennas, and an N5221A vector network analyzer is used to collect the scattering data.

The simulated and measured coefficient responses of the SAA and PCM-SAA are illustrated in Figure 11. It can be seen that the measured results roughly match the simulated ones. For the -10 dB impedance bandwidth, the SAA measures 11.23–11.75 GHz (4.5%), and the PCM-SAA measures 11.25–11.72 GHz (4.1%).

Figure 12 illustrates the simulated and measured normalized radiation patterns of the SAA and PCM-SAA at 11.5 GHz. It is obvious that the measured results agree well with the simulated ones. The results indicate that the radiation performance of the array antenna is well maintained after the incorporation of the PCM.

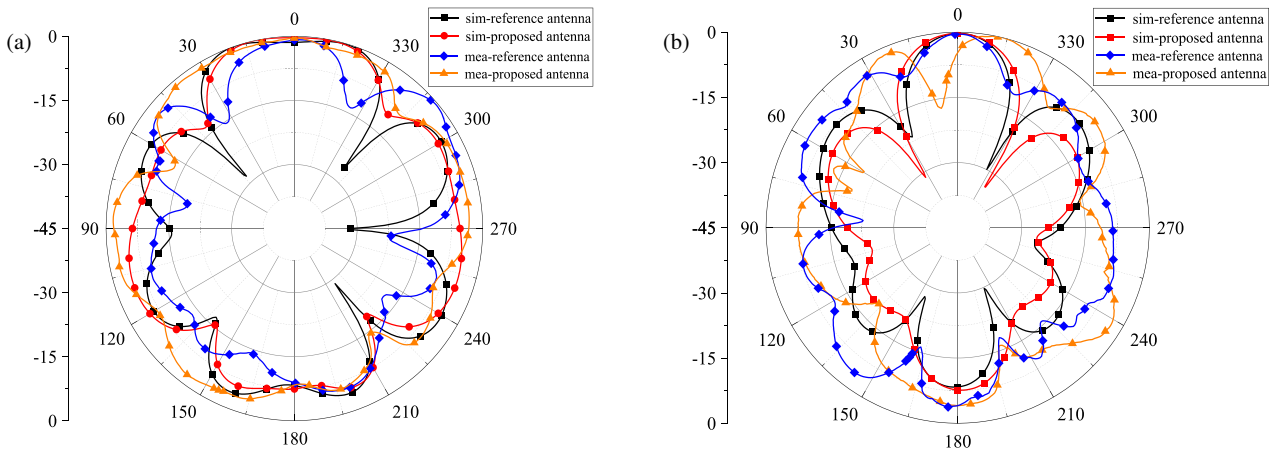

FIGURE 12. Normalized radiation patterns at 11.5 GHz. (a) SAA. (b) PCM-SAA.

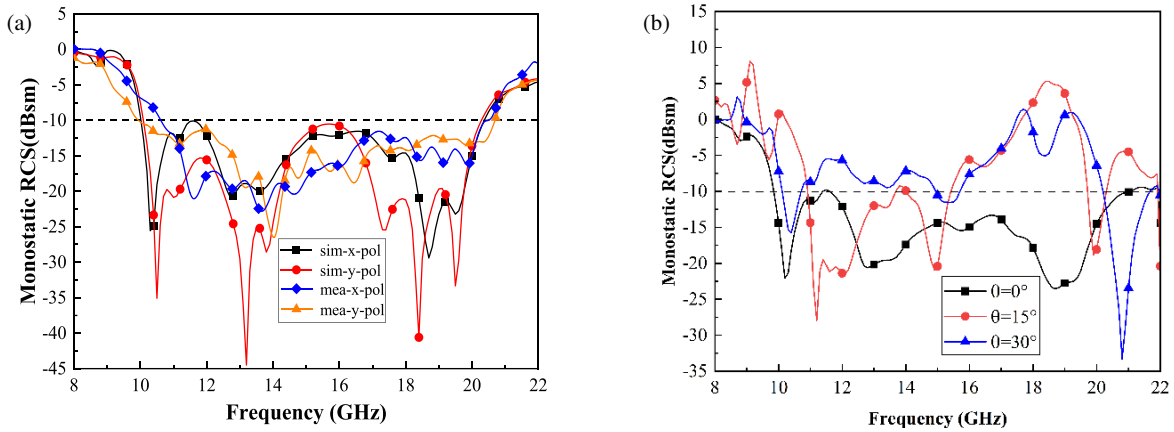

FIGURE 13. (a) Simulated and measured RCS reduction results of the antenna. (b) Simulated RCS of antenna under different incident angles.

TABLE 1. Performance comparison of low-RCS antennas.

Refs.	Size (λ_0^3)	Frequency (GHz)	10 dB RCSR BW (%)	IBW (%)	Max reduction (dB)
Ref. [18]	$1.15 \times 1.15 \times 0.029$	4.1–4.4	7.05	2.6	24
Ref. [19]	$1.54 \times 1.54 \times 0.06$	18–22.5	22.6	4.7	18
Ref. [20]	$1.67 \times 1.67 \times 0.145$	5.6–8	35.3	6.4	25
Ref. [21]	$1.21 \times 1.21 \times 0.07$	11.5–18	44	9.5	23
Ref. [22]	$1.62 \times 1.62 \times 0.05$	7.5–12	46	68	28
Ref. [23]	$2.22 \times 2.22 \times 0.259$	10–17	51.9	6.5	36
Ref. [24]	$4.55 \times 4.55 \times 0.09$	11.5–20	53.9	4.5	25
Ref. [25]	$1.49 \times 1.49 \times 0.18$	6–8	40	28.6	15
Ref. [26]	$1.25 \times 1.25 \times 0.66$	9–20	75.8	8.8	30
Ref. [27]	$1.35 \times 1.35 \times 0.05$	4.78–5.48	13.65	44.4	27.5
Ref. [28]	$18.14 \times 11.78 \times 0.134$	28.09–39.55	33.88	55.36	28.7
Proposed work	$2.39 \times 2.39 \times 0.127$	9.9–20.7	71.7	13.2	44

The simulated and measured monostatic RCS curves under normal incidence of the PCM-SAA are presented in Figure 13(a). It can be found that the measured scattering performance is roughly equal to the simulated results. The measured bandwidth of 10 dB RCS reduction ranges from 9.9 to 20.7 GHz (70.6%). Under x-polarized incidence, the maximum monostatic RCS reduction is 29 dB at 18.7 GHz. Meanwhile, under y-polarized incidence, the maximum monostatic RCS reduction reaches 44 dB at 13.2 GHz. The angular stability analysis is also conducted, and the simulated monostatic RCSs under different incident angles are illustrated in Figure 13(b). It is found that the effective RCS reduction bandwidth narrows gradually with increasing incident angle.

Finally, the comparison between the PCM-SAA and reported antennas is presented in Table 1. It can be seen that the PCM-SAA has the largest 10 dB RCS reduction bandwidth except for the antenna in [26]. Compared to the antenna in [26], the profile of the PCM-SAA in this work is reduced by 80.7%.

5. CONCLUSIONS

In this work, a low-profile PCM array antenna with broadband RCS reduction is presented. It consists of a slot antenna and a PCM array. The PCM-SAA achieves over 10 dB RCS reduction from 9.9 to 20.7 GHz (71.7%), and the maximum monostatic RCS reduction attains 29 dB at 18.7 GHz under x-polarized incidence and 44 dB at 13.2 GHz for y-polarized incidence. Notably, the PCM-SAA maintains effective radiation performance throughout.

ACKNOWLEDGEMENT

This work was partly supported by the National Natural Science Foundation of China (No. 6207128261771295), the Fundamental Research Program of Shanxi Province (No. 202303021221072), the Graduate Education Innovation Program Fund of Shanxi Province (No. 2025SJ064), and the Shanxi University's Training Program of Innovation for Undergraduates (No. X202510108364).

REFERENCES

[1] Costa, F. and A. Monorchio, "A frequency selective radome with wideband absorbing properties," *IEEE Transactions on Antennas and Propagation*, Vol. 60, No. 6, 2740–2747, 2012.

[2] El-Sewedy, M. F. and M. A. Abdalla, "A monostatic and bistatic RCS reduction using artificial magnetic conductor metasurface," *IEEE Transactions on Antennas and Propagation*, Vol. 71, No. 2, 1988–1992, 2023.

[3] Wang, Y., X. Ma, C. Guo, J. Ding, and X. Pang, "Ultra-wideband and wide-angle RCS reduction of antenna array using dual-layer miniaturized polarization conversion metasurface," *IEEE Antennas and Wireless Propagation Letters*, Vol. 24, No. 12, 4715–4719, 2025.

[4] Khan, H. A., J. Zhang, S. Luo, and Y. Wang, "A single-layer checkerboard metasurface based on reconfigurable polarization converter for dual-mode RCS reduction," *IEEE Antennas and Wireless Propagation Letters*, Vol. 24, No. 7, 2029–2033, 2025.

[5] Murugesan, A., K. T. Selvan, A. K. Iyer, K. V. Srivatsav, and A. Alphones, "A review of metasurface-assisted RCS reduction techniques," *Progress In Electromagnetics Research B*, Vol. 94, 75–103, 2021.

[6] Zaker, R. and A. Sadeghzadeh, "Passive techniques for target radar cross section reduction: A comprehensive review," *International Journal of RF and Microwave Computer-Aided Engineering*, Vol. 30, No. 11, e22411, 2020.

[7] Yu, W., M. Cheng, Y. Yu, W. Wang, L. Liu, and G. Q. Luo, "Bandpass absorptive frequency-selective structures with wide absorption bands based on hybrid 2-D and 3-D structures," *IEEE Transactions on Antennas and Propagation*, Vol. 71, No. 4, 3183–3192, 2023.

[8] Zhao, H., X. Zou, T. Liu, Y. Chen, R. Sun, C. Gao, F. Shi, Y. Liu, and Q. Feng, "High-gain-low-RCS PRS antenna with metasurface," in *2024 International Seminar on Artificial Intelligence, Computer Technology and Control Engineering (ACTCE)*, 167–171, Wuhan, China, Sep. 2024.

[9] Samadi, F. and A. Sebak, "Wideband, very low RCS engineered surface with a wide incident angle stability," *IEEE Transactions on Antennas and Propagation*, Vol. 69, No. 3, 1809–1814, 2021.

[10] Xi, Y., W. Jiang, K. Wei, T. Hong, T. Cheng, and S. Gong, "Wideband RCS reduction of microstrip antenna array using coding metasurface with low Q resonators and fast optimization method," *IEEE Antennas and Wireless Propagation Letters*, Vol. 21, No. 4, 656–660, 2022.

[11] Zhang, B., L. Li, C. Jin, Q. Lv, and R. Mittra, "Wideband low RCS antenna based on hybrid absorptive-diffusive frequency selective reflector," *IEEE Access*, Vol. 9, 77 863–77 872, 2021.

[12] Bandyopadhyay, B., S. Bhattacharya, R. K. Jaiswal, M. Saikia, and K. V. Srivastava, "Wideband RCS reduction of a linear patch antenna array using AMC metasurface for stealth applications," *IEEE Access*, Vol. 11, 127 458–127 467, 2023.

[13] Yang, R., X. Liao, Y. Wang, X. Qian, M. Wang, H. Zhang, and X. Fang, "Co-design of single-layer RCS-reducing surface and antenna array based on AMC technique," *Electronics*, Vol. 14, No. 12, 2392, 2025.

[14] Edalati, A. and K. Sarabandi, "Wideband, wide angle, polarization independent RCS reduction using nonabsorptive miniaturized-element frequency selective surfaces," *IEEE Transactions on Antennas and Propagation*, Vol. 62, No. 2, 747–754, 2014.

[15] Yang, L.-J., S. Sun, and W. E. I. Sha, "Ultrawideband reflection-type metasurface for generating integer and fractional orbital angular momentum," *IEEE Transactions on Antennas and Propagation*, Vol. 68, No. 3, 2166–2175, 2020.

[16] Yang, H., T. Li, J. Liao, K. Gao, Q. Li, S. Li, and X. Cao, "Ultrawideband low-RCS array antenna based on double-layer polarization conversion metasurface," *IEEE Antennas and Wireless Propagation Letters*, Vol. 23, No. 12, 4069–4073, 2024.

[17] Deng, G.-Y., Y.-H. Zhang, S.-Y. He, H. Yan, H.-C. Yin, H.-T. Gao, and G.-Q. Zhu, "Ultrabroadband RCS reduction design by exploiting characteristic complementary polarization conversion metasurfaces," *IEEE Transactions on Antennas and Propagation*, Vol. 70, No. 4, 2904–2914, 2022.

[18] Pazokian, M., N. Komjani, and M. Karimipour, "Broadband RCS reduction of microstrip antenna using coding frequency selective surface," *IEEE Antennas and Wireless Propagation Letters*, Vol. 17, No. 8, 1382–1385, 2018.

[19] Chen, Y., C. Xu, X. He, Y. Yang, H. Hu, and F. Li, "Stealth design of polarization conversion metasurface antenna array," *Microwave and Optical Technology Letters*, Vol. 63, No. 11, 2756–2762, 2021.

[20] Pandit, S., A. Mohan, and P. Ray, "Low-RCS low-profile four-element MIMO antenna using polarization conversion metasurface," *IEEE Antennas and Wireless Propagation Letters*, Vol. 19, No. 12, 2102–2106, 2020.

[21] Chatterjee, J., A. Mohan, and V. Dixit, "Radar cross section reduction and gain enhancement of slot antenna using polarization conversion metasurface for X-band applications," *International Journal of RF and Microwave Computer-Aided Engineering*, Vol. 31, No. 10, e22792, 2021.

[22] Li, Y., J. Jin, Z. Yang, J. Dou, H. Cheng, Y. Wang, and H. Yang, "Low-RCS low-profile MIMO antenna and array antenna using a polarization conversion metasurface," *Optics Express*, Vol. 31, No. 23, 38 771–38 785, 2023.

[23] Liu, Y., K. Li, Y. Jia, Y. Hao, S. Gong, and Y. J. Guo, "Wideband RCS reduction of a slot array antenna using polarization conversion metasurfaces," *IEEE Transactions on Antennas and*

Propagation, Vol. 64, No. 1, 326–331, 2016.

[24] Rahman, S. U., H. Deng, R. Li, H. Khalil, I. Khan, and H. Ullah, "Wideband radar cross section reduction of a circularly polarized antenna using polarization conversion metasurfaces," *Microwave and Optical Technology Letters*, Vol. 65, No. 7, 2048–2055, 2023.

[25] Luo, H., S. Wei, H. Zhang, K. Gong, and Q. Liu, "A C-band polarization conversion metasurface antenna with broadband RCS-reduction," *IEEE Antennas and Wireless Propagation Letters*, Vol. 24, No. 8, 2447–2451, 2025.

[26] Long, M., W. Jiang, and S. Gong, "Wideband RCS reduction using polarization conversion metasurface and partially reflecting surface," *IEEE Antennas and Wireless Propagation Letters*, Vol. 16, 2534–2537, 2017.

[27] Liu, W., R. Hong, Y. Qu, Q. Zheng, and X. Yang, "Wideband and low-RCS circularly polarized patch antenna based on polarization conversion metasurface using characteristic mode analysis," in *2022 International Conference on Microwave and Millimeter Wave Technology (ICMMT)*, 1–3, Harbin, China, Aug. 2022.

[28] Zhao, C., D. Shen, Y. Duan, Y. Wang, L. Luo, and L. Zhang, "A low-profile low-RCS dipole antenna based on bowtie-shaped polarization conversion metasurfaces," in *2025 IEEE MTT-S International Conference on Numerical Electromagnetic and Multiphysics Modeling and Optimization (NEMO)*, 1–3, Tianjin, China, 2025.

[29] Ren, J., W. Jiang, and S. Gong, "Low RCS and broadband metamaterial-based low-profile antenna using PCM," *IET Microwaves, Antennas & Propagation*, Vol. 12, No. 11, 1793–1798, 2018.

[30] Chen, H., J. Wang, H. Ma, S. Qu, Z. Xu, A. Zhang, M. Yan, and Y. Li, "Ultra-wideband polarization conversion metasurfaces based on multiple plasmon resonances," *Journal of Applied Physics*, Vol. 115, No. 15, 154504, 2014.